Available online at www.sciencedirect.com
SCIENCE DIRECT®
Journal of Sound and Vibration 268 (2003) 679–697
JOURNAL OF SOUND AND VIBRATION
www.elsevier.com/locate/jsvi

Parametric resonance of plates in a sheet metal coating process

C.H. Kim[a], N.C. Perkins[b], C.W. Lee[a,*]

[a] *Department of Mechanical Engineering, Center for Noise and Vibration Control (NoViC), Korea Advanced Institute of Science and Technology, Science Town, Daejeon 305-701, South Korea*

[b] *Mechanical Engineering and Applied Mechanics, The University of Michigan, Ann Arbor, MI 48109-2125, USA*

Received 11 February 2002; accepted 21 November 2002

Abstract

The vibration of sheet metal during zinc coating processes can lead to non-uniform coating thickness and overall poor product quality. This vibration develops from two principal mechanisms, namely, the run-out associated with the supporting rollers and/or bearings, and the time-varying tension associated with the manufacturing process. This study focuses on the second of these mechanisms (time-varying tension) that becomes significant under conditions leading to parametric resonance. The parametric resonance of the sheet metal is captured in a proposed model of a plate subject to time-varying and non-uniform edge tension. The model accounts for these effects as well as the non-linear stretching of the plate mid-plane as a result of transverse plate vibration. The linear vibration characteristics of the plate are studied first and are then used in deriving a single mode approximation of the non-linear, parametrically excited plate model. A perturbation solution of this model reveals the major parameters that influence parametric resonance in this application. Theoretical results for plate vibration are compared to experimental measurements of sheet metal vibration in a production facility. This comparison demonstrates that the model accurately captures the physical mechanisms responsible for sheet metal vibration and therefore, the physical parameters (such as damping) have the greatest impact on this vibration.

1. Introduction

The manufacturing of paper, film, plastic and sheet metal requires the handling of very thin and wide materials that are transported by rollers. The vibration of these materials or "plates" can adversely affect the quality of the finished product. For example, the zinc coating of steel sheet metal requires drawing the sheet through a bath of melted zinc and then drying the sheet in air

*Corresponding author. Tel.: +82-42-869-3016; fax: +82-42-869-8220.
E-mail address: cwlee@novic.kaist.ac.kr (C.W. Lee).

0022-460X/03/$ - see front matter
doi:10.1016/S0022-460X(02)01538-9

between two rollers as the zinc solidifies. In this process, the vibration of the sheet metal may lead to uneven zinc coating and poor product quality. The plate vibration derives from two principal mechanisms. The first mechanism is an external excitation that results from the eccentric rotation of the roller(s) and/or supporting bearings. Eccentric roller/bearing rotation produces motion normal to the sheet at the "boundary" formed by the roller. This excitation mechanism can be reduced by detuning the roller rotation frequency from any natural frequency of the sheet and/or by reducing roller eccentricity by frequent servicing/changing of the roller's bearings. The bearings experience rapid wear as they are also submerged in the zinc bath. The second mechanism is a parametric excitation that develops from the time varying tension experienced by the sheet metal plate. For instance, consider the experimental measurements of dynamic tension reported in Fig. 1(a). The magnitude of the time-varying tension is of the order of 10% of the mean tension, and it is a likely source of parametric resonance. The crowned shape of the roller also creates spatially varying tension in the width direction, and this is known to affect the linear vibration characteristics of wide plates [1]. This study focuses on the parametric resonance of plates by considering time-dependent, non-uniform tension, and non-linear mid-plane stretching.

Studies of plates, translating between two rollers, have considered many mechanical phenomena including plate vibration and wrinkling. The rollers are most frequently assumed to form either simply supported or clamped boundaries [1,2] while the two lateral edges are considered free. In cases where the plate tension is uniform, the linear plate vibration characteristics are well understood [3]. This understanding has also been extended to some cases of non-uniform plate tension. For instance, Ulsoy and Mote [1] evaluate the vibration of wide band saw blades subject to non-uniform edge tension applied at the roller/band interface. The membrane stresses produced by non-uniform edge tension have been computed using finite element [4] and Fourier series methods [2,5].

Time-dependent plate tension represents a source of parametric excitation and modelling this effect requires consideration of the mechanics of mid-plane stretching. Moreover, the analysis of

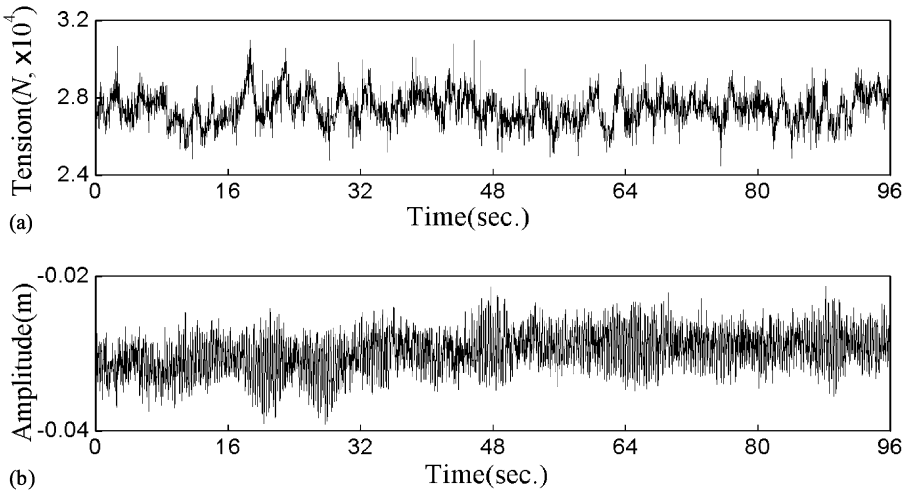

Fig. 1. Measured (a) tension and (b) vibration (displacement) data of plate in production sheet metal coating process ($v = 159$ m/min, $f_r = 3.52$ Hz).

finite amplitude vibrations of parametrically excited plates requires consideration of the non-linearities introduced by mid-plane stretching as captured in Von Karman plate theory [3,6]. Such models have extensively been used to evaluate the non-linear response of rectangular plates with all edges simply supported; see, for example, Refs. [7–11]. One-mode approximations for non-linear and parametrically excited plates lead to a parametrically excited Duffing oscillator as developed, for instance, in Refs. [11–13].

The objective of the present study is to extend our understanding of parametrically excited plate vibration by considering the effects of non-uniform and time-dependent tension for rectangular plates with two simply supported edges and two free edges. In addition, this study contributes an understanding of how parametric plate vibrations develop in the context of steel sheet metal processing. We begin by developing a model for this application.

2. Plate model

2.1. Non-linear plate equation of motion

Consider a thin, flat, rectangular plate of length L and width B moving between two rollers that form simple supports and that also provide tension as illustrated in Fig. 2, where $\hat{x}$, $\hat{y}$ and $\hat{z}$ are the co-ordinates. The tension applied at these boundaries is non-uniform in the width direction, in general. The two lateral sides of the plate are free. The thickness of the plate is h and the plate translation speed is v. For the motivating application (sheet metal forming), the translation speed is well below the critical speed $v_c = \sqrt{T_0/\rho B h}$ for a highly tensioned plate. Here, T_0 is the (spatially averaged) steady tension at the rollers, and ρ is the plate density. In particular, $v/v_c < 0.04$ for this application and the effects of the superimposed translation speed will therefore

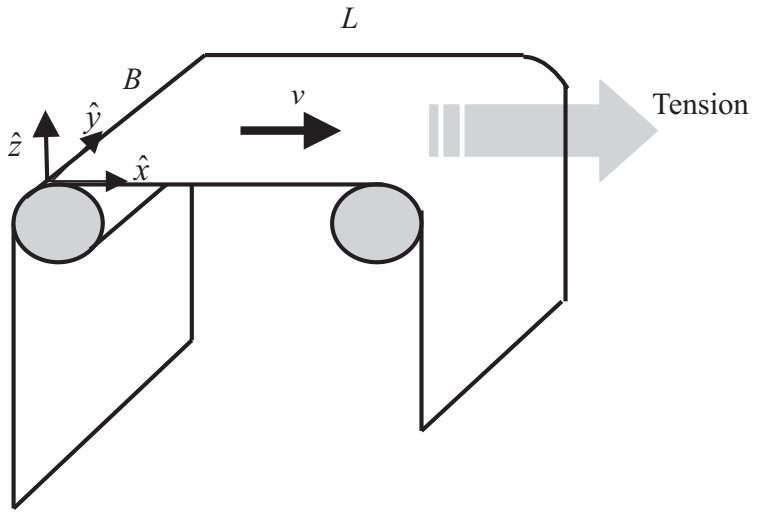

Fig. 2. Plate moving between two rollers with translation speed v subjected to tension.

be ignored [1]. The non-linear equations of motion capturing mid-plane stretching are [3,6]

$$\rho \frac{\partial^2 w}{\partial t^2} - \frac{\partial^2 F}{\partial y^2}\frac{\partial^2 w}{\partial x^2} + 2\frac{\partial^2 F}{\partial x \partial y}\frac{\partial^2 w}{\partial x \partial y} - \frac{\partial^2 F}{\partial x^2}\frac{\partial^2 w}{\partial y^2} + D\nabla^4 w = 0, \tag{1}$$

$$\nabla^4 F = Eh\left[\left(\frac{\partial^2 w}{\partial x \partial y}\right)^2 - \frac{\partial^2 w}{\partial x^2}\frac{\partial^2 w}{\partial y^2}\right], \tag{2}$$

where $w(x, y, t)$ is the transverse plate deflection (in the z direction), $D = Eh^3/[12(1-v^2)]$, E is Young's modulus, v is the Poisson ratio, and $\nabla^4 = \partial^4/\partial x^4 + 2\partial^4/\partial x^2 \partial y^2 + \partial^4/\partial y^4$ is the bi-harmonic operator. Here the co-ordinates x, y and w are normalized with respect to the span length L or $x = \hat{x}/L$, $y = \hat{y}/L$ and $w = \hat{w}/L$. $F(x, y, t)$ is an Airy stress function from which we compute the normal stress in the x direction T_x, the shear stress T_{xy}, and the normal stress in the y direction T_y using

$$T_x = \partial^2 F/\partial y^2, \quad T_y = \partial^2 F/\partial x^2, \quad T_{xy} = -2\partial^2 F/\partial x \partial y. \tag{3}$$

2.2. Natural frequencies and mode shapes under non-uniform tension

Consider next the equations of motion linearized about a pre-stressed state that is planar and created by applied, non-uniform tension at the two rollers. The Airy stress function for this equilibrium state satisfies $\nabla^4 F = 0$ subject to the following boundary conditions that define the conditions assumed at the rollers and free edges:

$$\begin{aligned} T_x(x, y) &= T(y) \text{ at } x = 0, 1, \\ T_y(x, y) &= 0 \text{ at } y = 0, s, \\ T_{xy}(x, y) &= 0 \text{ at } x = 0, 1 \text{ and } y = 0, s, \end{aligned} \tag{4}$$

Here, $s = B/L$ is the plate aspect ratio, and $T(y)$ is the prescribed non-uniform traction normal to the edge of the plate at the roller supports. For the special cases of rectangular plates subject to either *uniform or linearly* varying edge tension $T(y)$, the resulting stress components $T_y(x, y)$ and $T_{xy}(x, y)$ both vanish throughout the plate domain [2,14]. In all other cases, these stress components do not vanish and no exact solutions exist for their determination, in general. Approximate solutions can be determined using, for example, finite element [4] or Fourier series [2,5] methods. In this study, a modification of the methods employed in Refs. [2,5] is used to determine the stress distribution of a plate subject to a non-uniform edge tension that is *symmetrical* with respect to the center of the roller. A symmetric edge tension naturally arises in the motivating application due to the fact that the rollers are "crowned" (i.e., high in the middle). This edge tension is prescribed by

$$\begin{aligned} T_x(y) = K_1 \sin\left(\frac{\pi}{s}y\right) + \sum_{p=2,4}^{\tilde{p}} B_p \frac{1}{p\pi}\Big[D_{1p}(s)\cosh\left(p\pi\left(y - \frac{s}{2}\right)\right) \\ + D_{2p}(s)\left(y - \frac{s}{2}\right)\sinh\left(p\pi\left(y - \frac{s}{2}\right)\right)\Big], \quad \tilde{p} \to \infty, \end{aligned} \tag{5}$$

where the coefficients K_1, B_p may be selected to describe a specific symmetric tension distribution (boundary condition) and the functions $D_{1p}(s)$ and $D_{2\,p}(s)$ are defined in Appendix A. The functional form above leads to a simpler solution for the Airy stress function than that developed in Refs. [2,5] yet it is still dominated by the first (sinusoidal) term.

The resulting Airy stress function can be shown to be

$$F(x,y) = K_1 \sin\left(\frac{\pi}{s}y\right)\left[C_{11}\cosh\left(\frac{\pi}{s}\left(x-\frac{1}{2}\right)\right) + C_{21}\left(x-\frac{1}{2}\right)\sinh\left(\frac{\pi}{s}\left(x-\frac{1}{2}\right)\right)\right] + \left\{\sum_{p=2,4}^{\tilde{p}} B_p \cos(p\pi x)\left[D_{1p}(s)\cosh\left(p\pi\left(y-\frac{s}{2}\right)\right) + D_{2\,p}(s)\left(y-\frac{s}{2}\right)\sinh\left(p\pi\left(y-\frac{s}{2}\right)\right)\right]\right\}, \quad (6)$$

where the coefficients C_{11}, C_{21} are given in Appendix A. The associated stress components are illustrated in Fig. 3 for an example plate. As shown in Fig. 3, at the edges $x = 0, 1$, $T_x(x,y)$ satisfies

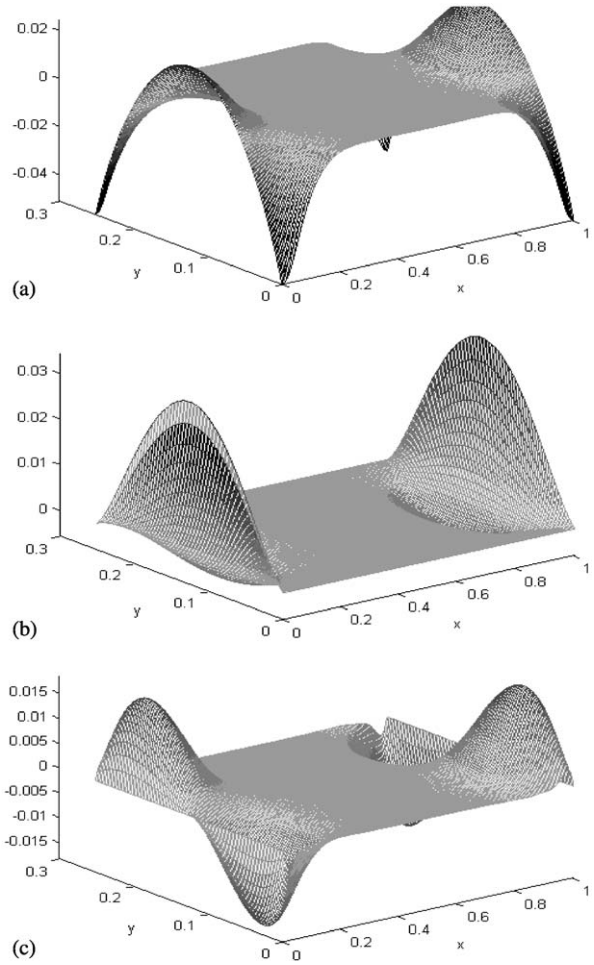

Fig. 3. Stress distributions under parabolic type of non-uniform tension. (a) $T_x(x,y)$, (b) $T_y(x,y)$ and (c) $T_{xy}(x,y)$. In this example, $s = 1/4$, $h/L = 8.7055 \times 10^{-5}$, $K_1 = T_0$ and $\tilde{p} = 10$.

Eq. (5) and resembles a symmetrical sine function. The boundary conditions $T_y(x, y) = 0$ at $y = 0, s$ and $T_{xy}(x, y) = 0$ at all edges are also satisfied. The overall spatial variations of these stress components resemble the results of Lin and Mote [2], for which the tension distribution for a sinusoidally varying edge tension was computed.

The linear transverse vibration characteristics of the plate, subject to the in-plane stresses above, are now evaluated using a standard Ritz series. The comparison functions in this series are selected to satisfy the assumed simply supported conditions at the rollers and the free conditions at the two lateral edges. The $m \times n$ separable Ritz series

$$W(x, y) = \sum_{j=0,k=1}^{m,n} a_{jk} Y_j(y) X_k(x), \tag{7}$$

for the eigenfunction W is formed in which a_{jk} represent unknown coefficients and $Y_j(y)$ and $X_k(x)$ are known comparison functions for a uniform beam satisfying simple–simple and free–free boundary conditions, respectively, as given in Appendix B [15].

The eigenvalue problem defining the plate natural frequencies and mode shapes is developed from the linear form of Eq. (1)

$$\bar{L}[W] = \lambda \bar{M}[W], \tag{8}$$

where $\lambda = \omega^2$ is an eigenvalue (ω is a natural frequency), and the linear operators $\bar{L}$ and $\bar{M}$ are given by

$$\bar{L} = -T_x \partial^2/\partial x^2 - T_y \partial^2/\partial y^2 - T_{xy} \partial^2/\partial x \partial y + D\nabla^4, \tag{9a}$$

$$\bar{M} = \rho. \tag{9b}$$

The operator $\bar{L}$ captures the dependence of the eigensolutions on the non-uniform edge tension through the in-plane stress components T_x, T_y and T_{xy}. Standard use of the Ritz method yields the plate natural frequencies and mode shapes that are briefly described below.

Consider first the effects of non-uniform edge tension on the plate natural frequencies and mode shapes. The non-uniform edge tension is illustrated in Fig. 4 and consists of a large mean tension $T_0 = 2.8$ ton with a small super-imposed parabolic variation in the width direction of magnitude T_2. Fig. 5 illustrates the variation of the lower natural frequencies with increasing non-uniformity (T_2/T_0) for four plates having distinct aspect ratios. The modes are distinguished by

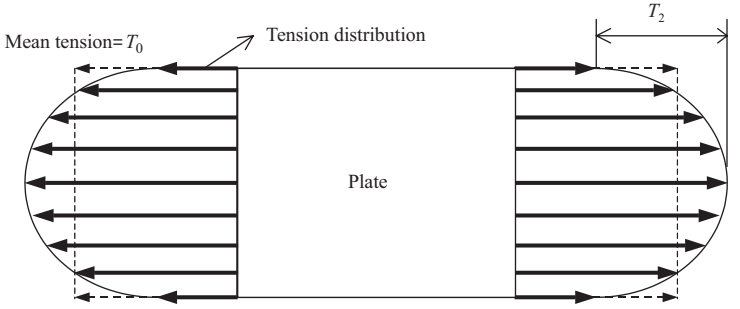

Fig. 4. Definition of a prescribed parabolic tension variation in the width direction.

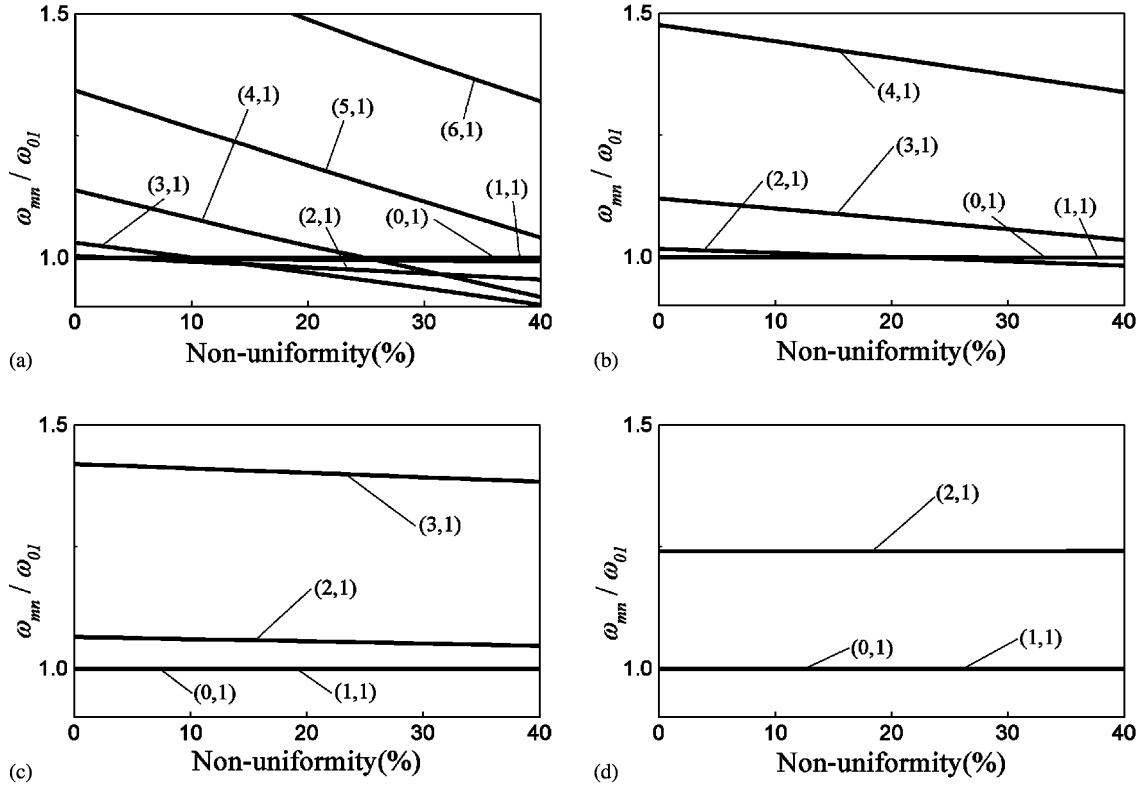

Fig. 5. Dependence of the natural frequencies of the lower vibration modes upon the non-uniformity of the tension. Non-uniformity refers to T_2/T_0, reported as a percentage. (a) $L = 2B$, (b) $L = 4B$, (c) $L = 8B$, and (d) $L = 16B$.

the indices (m, n) that denote the order of modes in the y and x directions, respectively, as defined in Appendix B. Note that as the plate aspect ratio (B/L) increases and the non-uniformity increases, the natural frequencies of the higher order modes ($m = 2, 3, 4$) decrease more rapidly than those of the two lower order modes ($m = 0, 1$). Moreover, the mode shapes for the higher order modes ($m = 2$, $n = 1$ and $m = 3$, $n = 1$) depend strongly upon the non-uniformity (T_2/T_0). For example, the mode W_{21} can, in general, be well represented by

$$W_{21} = (aY_0 + bY_2)X_1, \tag{10}$$

where the two parameters a and b are determined by the non-uniformity and the aspect ratio. The dependence of a and b on T_2/T_0 is shown in Fig. 6 for the case of $L = 4B$.

2.3. Discrete single-degree-of-freedom model for non-linear parametric vibration

The mode shapes discussed above are now used to develop a single-degree-of-freedom approximation for non-linear plate response. We begin first with discretizing the Airy function for the plate subject to non-uniform, time-varying tension and finite amplitude (non-linear) vibration.

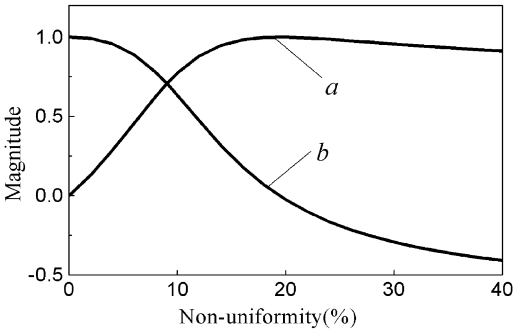

Fig. 6. Dependence of coefficients a and b upon the non-uniformity of the tension ($L = 4B$).

The Airy stress function can be decomposed into

$$F_{total}(x, y, t) = F(x, y) + F_{non}(x, y, t) + \tfrac{1}{2} r(t)(y - s/2)^2. \tag{11}$$

Here, $F(x, y)$ is the equilibrium (static) component as given by Eq. (6) and this captures the effects of the steady but non-uniform edge tension. The component $F_{non}(x, y, t)$ captures the additional mid-plane stresses developed by (non-linear) transverse vibration. Finally, the component $\frac{1}{2} r(t)(y - s/2)^2$ captures an assumed time variation of the mid-plane stresses due to a time-varying mean edge tension that is superimposed on the non-uniform edge tension. For instance, if the (spatial) mean edge tension varies as $T(t) = T_0 + \Delta T(t)$, then $r(t) = \Delta T(t)$. In this study, the time-dependent tension $\Delta T(t)$ will either be assumed to be harmonic or assumed known from experimental measurement. Attention now focuses on developing an expression for $F_{non}(x, y, t)$ from a single mode approximation of the vibration response.

Consider a single-degree-of-freedom approximation to the non-linear system (1) and (2) using a single mode of vibration as developed in Section 2.2 Thus, let

$$w(x, y, t) \approx W_{21} f(t) = (a Y_0 + b Y_2) X_1 f(t), \tag{12}$$

in which $f(t)$ is an unknown modal co-ordinate associated with the known vibration mode $W_{21}(x, y)$. This vibration mode is further described by the two parameters a and b introduced in Section 2.2 The associated Airy function must satisfy

$$\nabla^4 F_{non} = Eh[(\partial^2 w/\partial x \partial y)^2 - (\partial^2 w/\partial x^2)(\partial^2 w/\partial y^2)]. \tag{13}$$

Eq. (13) captures the non-linear stretching of the mid-plane of the plate provided the edges at the rollers are immovable. This later condition requires

$$u|_{x=0,1} = 0 \tag{14a}$$

with the remaining boundary conditions:

$$N_y = \partial^2 F_{non}/\partial x^2 = 0 \text{ at } y = 0, \text{s}, \tag{14b}$$

$$N_{xy} = -2\,\partial^2 F_{non}/\partial x \partial y = 0 \text{ at all edges}. \tag{14c}$$

At $x = 1$, Eq. (14a) can be re-written [6–11,13] as

$$u|_{x=1} = \int_0^1 (\varepsilon_x - \tfrac{1}{2}(\partial w/\partial x)^2)\,\mathrm{d}x = \int_0^1 [(N_x - \nu N_y)/Eh - \tfrac{1}{2}(\partial w/\partial x)^2]\,\mathrm{d}x. \tag{15}$$

Substituting Eq. (12) into Eq. (13) gives

$$\begin{aligned}\nabla^4 F_{non}/Eh = f^2(t)[a^2(X_1' Y_0' X_1' Y_0' - X_1'' Y_0 X_1 Y_0'') + b^2(X_1' Y_2' X_1' Y_2' - X_1'' Y_2 X_1 Y_2'') \\ + ab(2X_1' Y_0' X_1' Y_2' - X_1'' Y_0 X_1 Y_2'' - X_1'' Y_2 X_1 Y_0'')],\end{aligned} \tag{16}$$

where $X_1' = \partial X_1/\partial x$, $X_1'' = \partial^2 X_1/\partial x^2$ and $Y_m' = \partial Y_m/\partial y$, $Y_m'' = \partial^2 Y_m/\partial y^2$ for $m = 0, 2$. F_{non} can now be decomposed as

$$F_{non} = f^2(t)[a^2 F_{aa}(x,y) + abF_{ab}(x,y) + b^2 F_{bb}(x,y)], \tag{17}$$

where the spatial functions F_{aa}, F_{ab} and F_{bb} are evaluated using the procedure in Appendix C. From the total Airy function given by Eq. (11), the associated stress distributions are

$$\begin{aligned} T_x^{total} &= \partial^2 F_{total}/\partial y^2 = T_x + N_x^* f^2(t) + r(t), \\ T_y^{total} &= \partial^2 F_{total}/\partial x^2 = T_y + N_y^* f^2(t), \\ T_{xy}^{total} &= -2\partial^2 F_{total}/\partial x \partial y = T_{xy} + N_{xy}^* f^2(t), \end{aligned} \tag{18}$$

where $N_x^* = N_x/f^2(t)$, $N_y^* = N_y/f^2(t)$, and $N_{xy}^* = N_{xy}/f^2(t)$.

Standard use of Galerkin's method using Eq. (12) in Eqs. (1) and (2) leads to the single non-linear equation governing the modal co-ordinate $f(t)$:

$$\ddot{f}(t) + 2\varsigma\omega_0 \dot{f}(t) + [\alpha + \gamma_\varepsilon r(t)] f(t) + \beta_\varepsilon f^3(t) = 0, \tag{19}$$

where α, β_ε, γ_ε are given in Appendix D and ω_0 is the natural frequency of the mode considered. Note that $\alpha = \omega_0^2$ and that modal damping ς has been added.

3. Analysis of parametric resonance

Assume that the time-varying tension is described by the single harmonic

$$r(t) = \cos \omega t. \tag{20}$$

Analysis of the linearized form of (19) will provide the stability boundaries that separate stable from unstable trivial solutions. Subsequent analysis of the non-linear form will be used to assess the limit cycles that bifurcate from the trivial solution.

3.1. Linear system

Substitution of Eq. (20) into Eq. (19) and elimination of the non-linear term yields

$$\ddot{f} + 2\varsigma\omega_0 \dot{f} + (\omega_0^2 + \gamma_\varepsilon \cos \omega t) f = 0, \tag{21}$$

in which ε is small, non-dimensional small parameter defined by $\varepsilon = h/L$. Letting $2\varsigma\omega_0 = 2C\varepsilon$, $\gamma_\varepsilon = 2\varepsilon\gamma$ in Eq. (21) produces

$$\ddot{f} + 2C\varepsilon\dot{f} + (\omega_0^2 + 2\varepsilon\gamma\cos\omega t)f = 0. \tag{22}$$

The solution of Eq. (22) can be represented by the first order multiple-scales expansion [13]

$$f = f_0(\tau_0, \tau_1) + \varepsilon f_1(\tau_0, \tau_1), \tag{23}$$

where $\tau_n = \varepsilon^n t$ for $n = 0, 1$. This expansion is used to evaluate the (principal) parametric resonance centered about $\omega = 2\omega_0$. Letting $\omega = 2\omega_0 + \varepsilon\sigma$, where σ is a detuning parameter, and using a standard multiple scales analysis [13] leads to the instability boundaries

$$-\sqrt{\gamma^2/\omega_0^2 - 4C^2} < \sigma < \sqrt{\gamma^2/\omega_0^2 - 4C^2}. \tag{24}$$

The trivial solution is unstable for values of the detuning parameter between these bounds. As expected, non-trivial periodic solutions bifurcate from the trivial solution at the stability boundaries as seen in the following analysis of the non-linear system.

3.2. Non-linear system

The non-linear parametrically excited plate is governed by

$$\ddot{f} + 2C\varepsilon\dot{f} + (\omega_0^2 + 2\varepsilon\gamma\cos\omega t)f + \varepsilon\beta f^3 = 0, \tag{25}$$

where $\beta = \beta_\varepsilon / \varepsilon$. The zeroth order solution is written as

$$f_0 = A(\tau_1)\mathrm{e}^{\mathrm{i}\omega_0\tau_0} + \bar{A}(\tau_1)\mathrm{e}^{-\mathrm{i}\omega_0\tau_0}, \tag{26}$$

and it captures modulations on the τ_1 time scale. Introduce the polar form

$$A(\tau_1) = \tfrac{1}{2}a_A(\tau_1)\mathrm{e}^{\mathrm{i}\phi(\tau_1)}, \tag{27}$$

where $a_A(\tau_1)$ and $\phi(\tau_1)$ denote a slowly varying amplitude and phase, respectively. Steady solutions for a_A and ϕ provide the amplitude and phase of a periodic solution to Eq. (25). The steady amplitude obeys [13]

$$\{C^2 + (\tfrac{1}{2}\sigma a_A - \tfrac{3}{8}\beta a_A^2/\omega_0)^2\}a_A^2 = \tfrac{1}{4}\gamma^2 a_A^2/\omega_0^2. \tag{28}$$

Thus, the trivial solution ($a_A^2 = 0$) is always a solution, and the non-trivial solutions are given by

$$(\tfrac{3}{8}\beta/\omega_0)a_A^2 = \tfrac{1}{2}\sigma \pm \sqrt{\tfrac{1}{4}\gamma^2/\omega_0^2 - C^2}, \tag{29}$$

provided

$$(\tfrac{3}{8}\beta/\omega_0)a_A^2 = \tfrac{1}{2}\sigma \pm \sqrt{\tfrac{1}{4}\gamma^2/\omega_0^2 - C^2} > 0. \tag{30}$$

The stability of these non-trivial solutions may also be assessed by evaluating the eigenvalues of the amplitude and phase modulation equations after linearization about a known periodic solution. The stability depends upon the excitation amplitude parameter γ and the detuning parameter σ. Three distinct types of behaviors are found as illustrated in Fig. 7 [13]. In region I, only the trivial solution exists and it is stable. Thus, the response from any initial condition decays

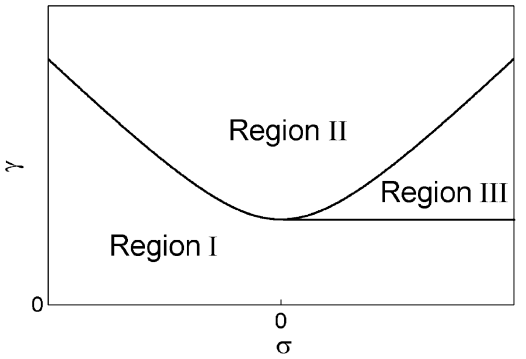

Fig. 7. Three regions that determine qualitatively distinct behaviors of periodic response [13].

to zero as also predicted by the linear system. In region II, a stable non-trivial solution as well as the unstable trivial solution co-exist so that all initial conditions produce a limit cycle. In region III, the trivial solution regains stability and the two non-trivial solutions co-exist; one stable (larger amplitude) and the other unstable (smaller amplitude). As a result, solutions always decay to zero or converge to the stable solution whose amplitude is computed from $(\frac{3}{8}\beta/\omega_0)a_A^2 = \frac{1}{2}\sigma + \sqrt{\frac{1}{4}\gamma^2/\omega_0^2 - C^2}$. Thus, in this region, two stable periodic solutions co-exist and the initial conditions ultimately determine which of these two periodic motions represent the long-term response.

4. Parametric resonance in sheet metal coating process

An example sheet metal coating process is studied that reveals the importance of parametric resonance in producing vibrations of the sheet metal. These vibrations in turn may lead to variations in coating thickness that can degrade the quality of the finished product.

A schematic of this process is shown in Fig. 2 where the plate of steel sheet metal is covered with molten zinc that solidifies as the plate translates between the two rollers shown. The plate has dimensions $L = 22.5\,\text{m}$ (length), $B = 1.209\,\text{m}$ (width), and $h = 0.421\,\text{mm}$ (thickness), and it translates with speeds ranging from $v = 140$ to $180\,\text{m/min}$.

Fig. 1(b) illustrates the measured displacement of the plate sampled using a proximity sensor that is located at 1 m from the roller that is submerged in the zinc bath and also at the centerline of the plate (sensor location: $x = 1/22.5$, $y = 1.209/45$). The time record shown is for a period of 96 s. The data were then analyzed by computing the harmonic wavelet [16]. The resulting time-frequency map is illustrated in Fig. 8. Apparent at all times is a pronounced peak at $f_r = 3.52\,\text{Hz}$ that corresponds to the rotation frequency of the two rollers. Thus, it is clear that the rollers are responsible for the majority of the plate vibration and this derives from roller and/or bearing run-out. Moreover, a secondary peak at twice the roller frequency is often present. Also observable is a peak at the fundamental natural frequency of the plate $f_n = 3.69\,\text{Hz}$ in Case B (from 16 to 32 s), Case D (from 43 to 53 s) and Case F (from 83 to 96 s) that show large peaks and Case C (32 to 43 s), Case E (53 to 83 s) that show small peaks. This sustained response at the natural frequency is expected when the plate is parametrically excited as discussed next.

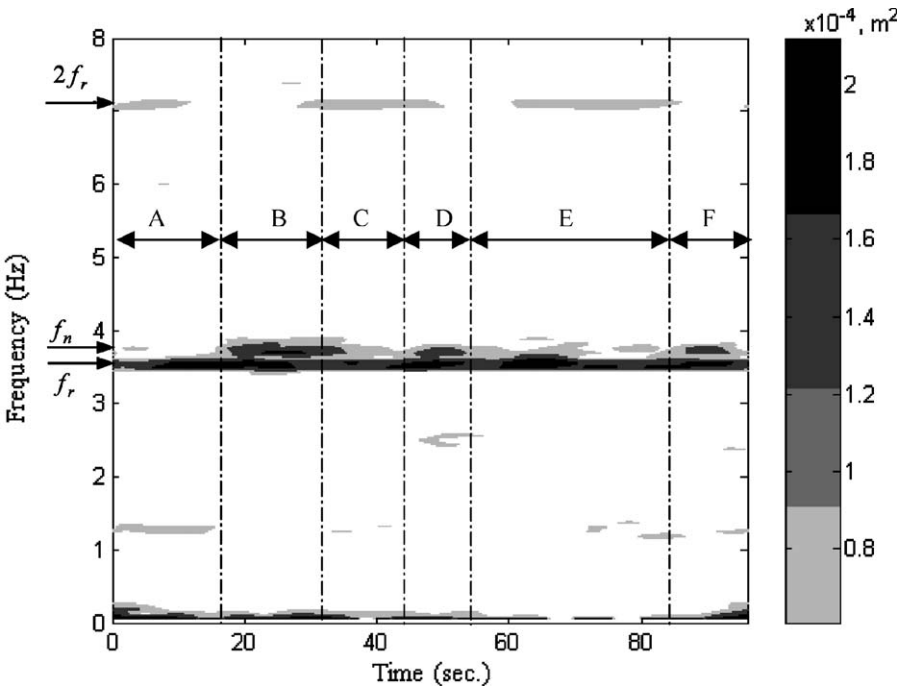

Fig. 8. Time–frequency map of vibration data in Fig. 1(b).

The likely source of parametric excitation is the time-dependent tension that develops in this process due to multiple mechanisms including unsteady process speed, unsteady roller dynamics, roller/bearing run-out, and the like. The fundamental vibration mode may experience parametric resonance when these tension fluctuations are reasonably significant and also occur at frequencies near to twice the fundamental natural frequency. To investigate this, data for dynamic tension were collected using a roller instrumented with load cells to measure bearing reactions, hence dynamic tension. Fig. 9 shows the harmonic wavelet map of the dynamic tension data given in Fig. 1(a). The frequency range of $2f_n \pm 0.15 = 7.38 \pm 0.15$ Hz is identified by two dashed lines. Note that, although the dynamic tension data have a wide range of frequency components, their contributions, except the identified frequency range, to the response are insignificant as shown in Fig. 8. The greatest amount of dynamic tension in this range occurs for Cases B, D and F. In each of these cases, there is a significant corresponding peak at f_n in Fig. 8. In addition, Cases A (0–16), C and E in Fig. 9 have dynamic tension peaks in this range but narrower and smaller than Cases B, D and F, thus there are very small peaks at f_n in Cases C and E and no peak in Case A of Fig. 8.

The model and analysis of Section 3 may be used to estimate the magnitude of the plate vibration due to parametric resonance for the experimental conditions described above. To this end, we shall focus on Case A (no observable parametric resonance) and B (clearly observable parametric resonance) beginning with an estimate of the magnitude of the dynamic tension for both cases. This estimate may be obtained from the power spectra in Figs. 10(a) and (b) which are the power spectra of the tension data of Cases A and B, respectively, and which lead to

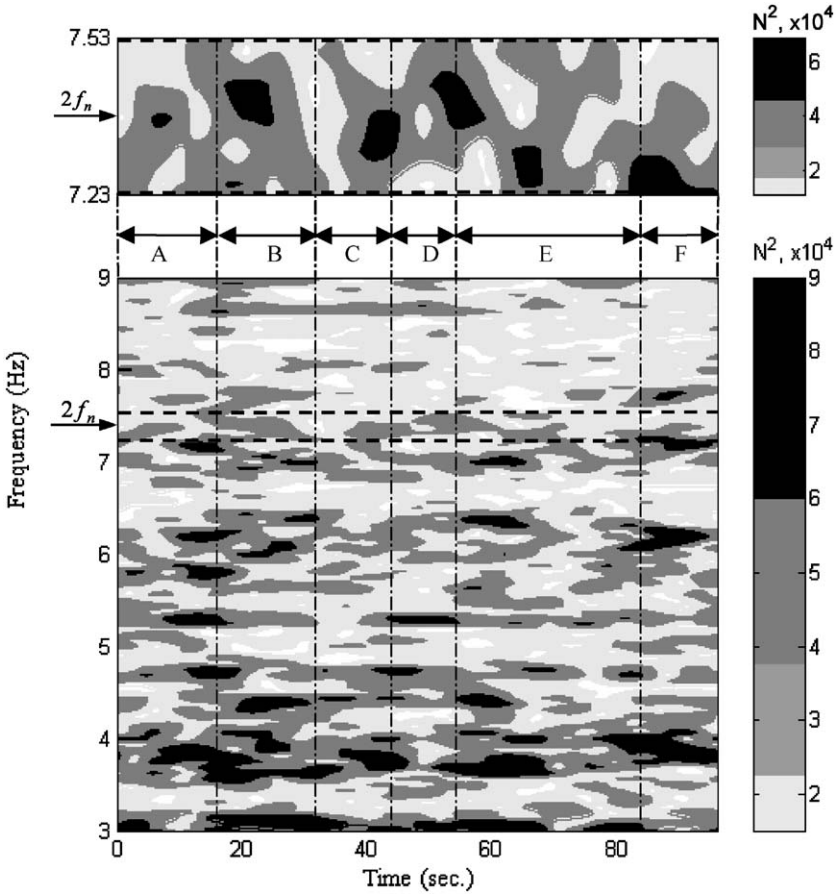

Fig. 9. Time–frequency map of tension data of Fig. 1(a).

$\Delta T/T_0 = 0.53\%$ for Case A and $\Delta T/T_0 = 0.89\%$ for Case B. The coefficients β and γ in Eq. (25) are 3.42×10^9 and 1.51×10^5 for Case A, and $\gamma = 2.54 \times 10^5$ for Case B. The damping ratio ς is an unknown but important factor in determining whether the parametric resonance exists. This is clearly seen in Fig. 11 that shows how the stability boundary depends upon the damping ratio in the range from 0.002 to 0.005. Consider the case of $\varsigma = 0.003$ and zero detuning $\sigma = 0$. For Case A, $\gamma = 1.51 \times 10^5$ which places this case within the stable region for the trivial solution and no parametric resonance is expected. By contrast, for Case B, $\gamma = 2.54 \times 10^5$, and this falls well within the unstable region for the trivial solution and a stable (non-trivial) periodic solution exists. Should the damping ratio actually be as large as $\varsigma = 0.005$, then Case B lies in the stable region for the trivial solution and no parametric resonance would be observed. Likewise, should the damping decrease to $\varsigma = 0.002$, then Case A lies in the unstable region and parametric resonance would then be observable. Thus the damping ratio has an expected and pronounced effect on the parametric resonance.

For the purpose of illustration, consider again the case $\varsigma = 0.003$ and the response of the plate due to both parametric and external excitation as predicted by the non-linear single-degree-of-

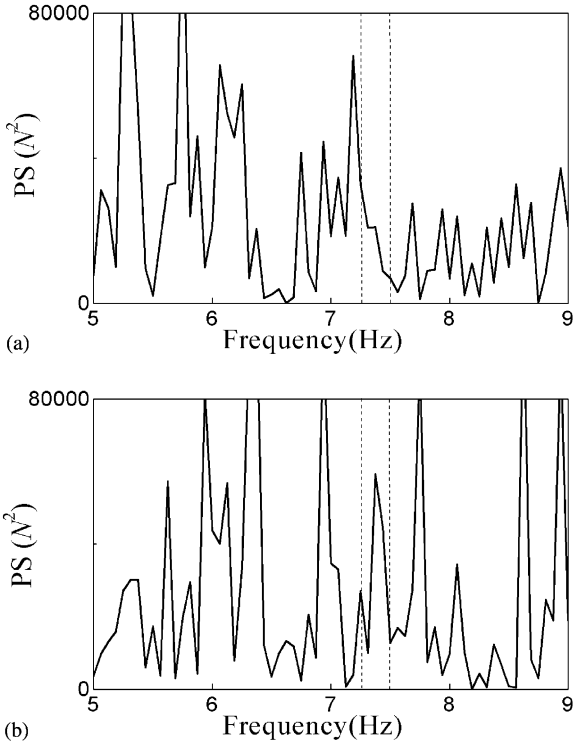

Fig. 10. Power spectra obtained from the measured tension for (a) Case A, and (b) Case B.

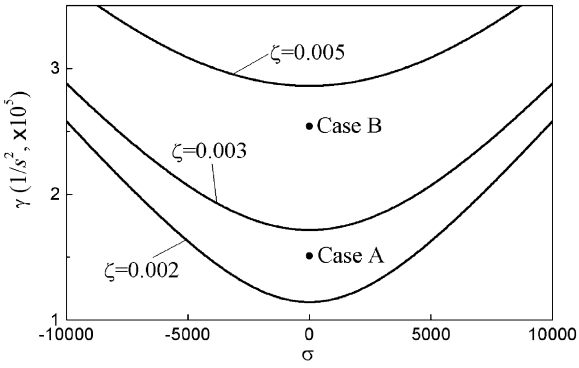

Fig. 11. Dependence of stability boundary on the damping.

freedom model

$$\ddot{f} + 2\varsigma\omega_0\dot{f} + R(t)f + \beta_\varepsilon f^3(t) = \ddot{q}_e(t). \tag{31}$$

Here, $R(t) = \int_{D^*}(-T(t)\partial^2 W/\partial x^2 + DW\nabla^4 W)\,\mathrm{d}D^* / \int_{D^*}\rho W^2\,\mathrm{d}D^*$, D^* is the integration domain, $T(t)$ is the recorded tension data from the sheet metal coating experiment as given in Fig. 1(a), and $q_e(t) = Q_e\cos(\omega_r t)$ represents an assumed harmonic moving boundary excitation due to roller

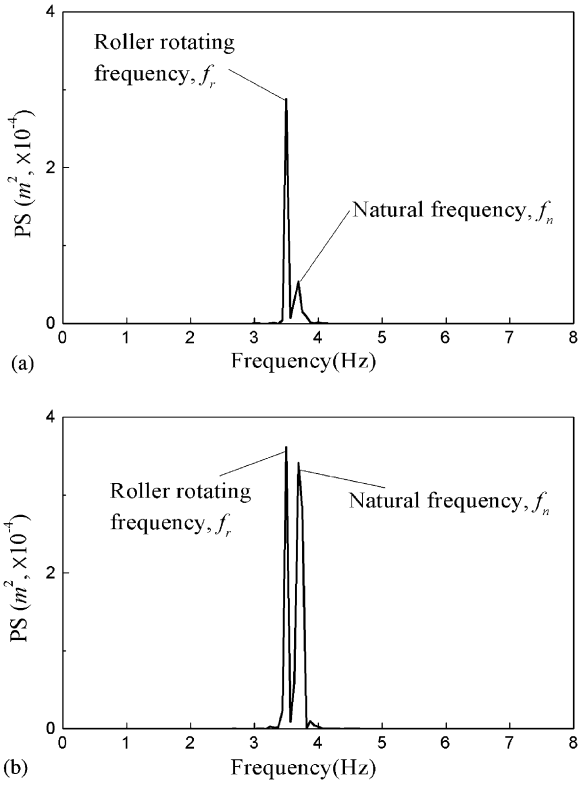

Fig. 12. Power spectra obtained from model for (a) Case A, and (b) Case B.

eccentricity of amplitude Q_e and frequency $\omega_r = 2\pi f_r$. The amplitude Q_e is unknown but can be estimated from the measured plate response data. Direct numerical integration of Eq. (31) for Cases A and B leads to the computed response power spectra shown in Figs. 12(a) and (b), respectively.

To arrive at these results, we adjusted one parameter, namely the (unknown) magnitude of the eccentricity Q_e. In particular, Q_e was tuned to minimize the error between the measured (Fig. 13) and the predicted (Fig. 12) response power spectra. These results demonstrate that the response for Case A is dominated by the roller eccentricity while the response for Case B is nearly equally partitioned between the roller eccentricity and parametric resonance. Moreover, the overall agreement between the measured and predicted power spectra is very good.

5. Summary and conclusions

A non-linear model is proposed for describing the parametric resonance of a plate subject to non-uniform and time-varying edge tension. A one mode approximation of the response is used to develop a non-linear single-degree-of-freedom model that is analyzed using a perturbation

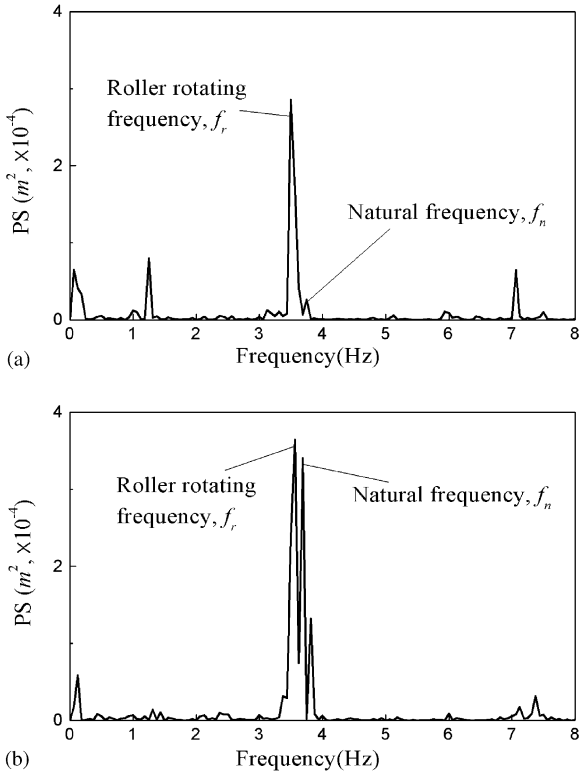

Fig. 13. Power spectra obtained from the measured response for (a) Case A, and (b) Case B.

method. This analysis reveals the conditions under which the plate is likely to experience principal parametric resonance of its fundamental mode due to time-varying tension. This theory is then used to explain experimental results for sheet metal vibration in a production sheet metal coating process.

Analysis of the experimental data reveals that sheet metal vibration originates from two major mechanisms: (1) external excitation due to roller/bearing run-out, and (2) parametric excitation due to time-varying tension. Measurements of the time-varying tension confirm the existence of frequency components at twice the fundamental natural frequency of the plate. Measurements of plate vibration confirm predictions from the theoretical model that the measured time-varying tension is sufficient to generate plate parametric resonance. In this case, the model also reveals that the parametric resonance is strongly influenced by the plate damping. Finally, increasing plate damping may provide a means to eliminate the parametric resonance in this application.

Acknowledgements

The authors are grateful to Pohang Iron & Steel Co., Ltd. for financial support of the research. This work was also supported by the Brain Korea 21 project.

Appendix A

$$C_{11} = -\frac{2s^2[\sinh(\pi/2s) + (\pi/2s)\cosh(\pi/2s)]}{\pi^2[\pi/s + \sinh(\pi/s)]}, \quad C_{21} = \frac{2s\sinh(\pi/2s)}{\pi[\pi/s + \sinh(\pi/s)]}$$

$$D_{1p} = \frac{s\sinh(p\pi s/2)}{p\pi[p\pi s + \sinh(p\pi s)]}, \quad D_{2p} = -\frac{s\cosh(p\pi s/2)}{p\pi[p\pi s + \sinh(p\pi s)]}.$$

Appendix B

$$X_k(x) = \sin k\pi x, \ \ \mathrm{k} = 1, 2, \ldots, \tag{B.1}$$

$$Y_0(y) = A_0, \tag{B.2}$$

$$Y_1(y) = A_1(y - s/2), \tag{B.3}$$

$$Y_j(y) = A_j[\sin(\beta_j y/s) + \sinh(\beta_j y/s)] + B_j[\cos(\beta_j y/s) + \cosh(\beta_j y/s)], \ \ j = 2, 3, 4, \ldots, \tag{B.4}$$

where $A_j = \cos\beta_j - \cosh\beta_j$, $B_j = -(\sin\beta_j - \sinh\beta_j)$ and $\cos\beta_j \cosh\beta_j = 1$. Note that Eqs. (B.2) and (B.3) describe the two rigid-body modes of a free–free beam.

Appendix C

Using $N_x = \partial^2 F_{non}/\partial y^2$, $N_y = \partial^2 F_{non}/\partial x^2$ and substituting Eqs. (12) and (17) into Eq. (15) leads to

$$\begin{aligned}\frac{1}{Eh}(N_x - vN_y) - \frac{1}{2}\left(\frac{\partial w}{\partial x}\right)^2 = f^2(t)\Bigg[a^2\left(\frac{\partial^2 F_{aa}}{Eh\partial y^2} - v\frac{\partial^2 F_{aa}}{Eh\partial x^2} - X_1'^2 Y_0^2\right) \\ + b^2\left(\frac{\partial^2 F_{bb}}{Eh\partial y^2} - v\frac{\partial^2 F_{bb}}{Eh\partial x^2} - X_1'^2 Y_2^2\right) \\ + ab\left(\frac{\partial^2 F_{ab}}{Eh\partial y^2} - v\frac{\partial^2 F_{ab}}{Eh\partial x^2} - X_1'^2 Y_0 Y_2\right)\Bigg].\end{aligned} \tag{C.1}$$

Next, we separate terms having constant coefficients and terms proportional to a^2, b^2 and ab. Consider a particular solution F_{bb}^p that satisfies

$$\nabla^4 F_{bb}^p/Eh = f^2(t)[b^2(X_1' Y_2' X_1' Y_2' - X_1'' Y_2 X_1 Y_2'')]. \tag{C.2}$$

F_{bb}^p can be written as

$$F_{bb}^p = (\cos 2\pi x) g_{bb}(y) + h_{bb}(y), \tag{C.3}$$

where $g_{bb}(y)$ and $h_{bb}(y)$ are functions of y. However, the stress distributions from Eq. (C.3) do not satisfy conditions (2.14b) and (2.14c), but do satisfy $N_{bbxy}^p|_{x=0,1} = 0$ as required. Consider an Airy

function F_{bb}^h given by

$$F_{bb}^h = [C_{bb}^{h1}\cosh\{2\pi(y-s/2)\} + C_{bb}^{h2}(y-s/2)\sinh\{2\pi(y-s/2)\}]\cos 2\pi x + [D_{bb}^{h1}\cosh\{2\pi(y-s/2)\} + D_{bb}^{h2}(y-s/2)\sinh\{2\pi(y-s/2)\}]\ \cos 2\pi x, \tag{C.4}$$

that satisfies the homogeneous equation $\nabla^4 F_{bb}^h = 0$. The first term, denoted F_{bb}^{h1}, when added to a term of the particular solution $F_{bb} = F_{bb}^p + F_{bb}^h$ satisfies $\partial^2 F_{bb}/\partial x^2|_{y=0,s} = 0$ by selection of the coefficients C_{bb}^{h1}, C_{bb}^{h2} and this guarantees $\partial^2 F_{bb}^{h1}/\partial x\partial y|_{x=0,1\&y=0,s} = 0$. The second term, denoted F_{bb}^{h2}, when added to a term of the particular solution $F_{bb} = F^p_{bb} + F^h_{bb}$ satisfies $\partial^2 F_{bb}/\partial x\partial y|_{y=0,s} = 0$ by selection of the coefficients D_{bb}^{h1}, D_{bb}^{h2} and this guarantees $\partial^2 F_{bb}^{h2}/\partial^2 x|_{y=0,s} = 0$. Thus F_{bb} that satisfies the boundary conditions for the stresses is

$$F_{bb} = F_{bb}^p + F_{bb}^h. \tag{C.5}$$

It can easily be shown that

$$\int_0^1 \left(\frac{\partial^2 F_{bb}}{Eh\partial y^2} - v\frac{\partial^2 F_{bb}}{Eh\partial x^2} - X_1'^2 Y_2^2\right) \mathrm{d}x = 0. \tag{C.6}$$

By similar procedure, F_{ab} satisfying $\nabla^4 F_{ab}/Eh = f^2(t)ab(-X_1'' Y_0 X_1 Y_2'')$ can also be found. Let

$$F_{ab} = F^p_{ab} + F^h_{ab}, \tag{C.7}$$

where F_{ab}^p is given by Eq. (C.8) and F_{ab}^h is the homogeneous solution that allows F_{ab} to satisfy the boundary conditions. The particular solution is

$$F_{ab}^p = (\cos 2\pi x)g_{ab}(y) + h_{ab}(y), \tag{C.8}$$

where $g_{ab}(y)$ and $h_{ab}(y)$ are also functions of y. In this case,

$$\int_0^1 \left(\frac{\partial^2 F_{ab}}{Eh\partial y^2} - v\frac{\partial^2 F_{ab}}{Eh\partial x^2} - X_1'^2 Y_0 Y_2\right) \mathrm{d}x = 0. \tag{C.9}$$

Finally, F_{aa} which satisfies $\nabla^4 F_{aa}/Eh = 0$ is

$$F_{aa} = \frac{Eh}{8} Y_0^2 \pi^2 f^2(t)(y - s/2)^2, \tag{C.10}$$

from which

$$\int_0^1 \left(\frac{\partial^2 F_{aa}}{Eh\partial y^2} - v\frac{\partial^2 F_{aa}}{Eh\partial x^2} - X_1'^2 Y_0^2\right) \mathrm{d}x = 0. \tag{C.11}$$

This method described above can be applied to all vibration modes that consisted of Y_0X_1 and Y_2X_1 including $W_{01} = Y_0X_1$ and $W_{21} = Y_2X_1$.

Appendix D

Let

$$A_W = \int_0^s \int_0^1 \left(-T_x W\frac{\partial^2 W}{\partial x^2} - T_y W\frac{\partial^2 W}{\partial y^2} + T_{xy} W\frac{\partial^2 W}{\partial x\partial y} + DW\nabla^4 W\right) \mathrm{d}x\,\mathrm{d}y, \tag{D.1}$$

$$B_W = \int_0^s \int_0^1 \left(-N_x^* W \frac{\partial^2 W}{\partial x^2} - N_y^* W \frac{\partial^2 W}{\partial y^2} + N_{xy}^* W \frac{\partial^2 W}{\partial x \partial y} \right) \mathrm{d}x \, \mathrm{d}y, \tag{D.2}$$

$$C_W = \int_0^s \int_0^1 \left(-\Delta T W \frac{\partial^2 W}{\partial x^2} \right) \mathrm{d}x \, \mathrm{d}y, \tag{D.3}$$

$$G = \int_0^s \int_0^1 W \bar{M}[W] \, \mathrm{d}x \, \mathrm{d}y = \rho \int_0^s \int_0^1 W^2 \, \mathrm{d}x \, \mathrm{d}y. \tag{D.4}$$

Then the coefficients

$$\alpha_\varepsilon = \frac{A_W}{G} = \omega_0^2, \tag{D.5}$$

$$\beta_\varepsilon = \frac{B_W}{G}, \tag{D.6}$$

$$\gamma_\varepsilon = \frac{C_W}{G}. \tag{D.7}$$

References

[1] A.G. Ulsoy, C.D. Mote Jr., Vibration of wide band saw blades, Journal of Sound and Vibration 104 (1982) 71–78.
[2] C.C. Lin, C.D. Mote Jr., The wrinkling of rectangular webs under non-linearly distributed edge loading, Journal of Applied Mechanics 63 (1996) 655–659.
[3] A.W. Leissa, Vibration of Plates, NASA-Sp-160, 1969.
[4] J.E. Borchelt, A.G. Ulsoy, P. Papalambros, Efficient computation of band saw blade stresses, Journal of Mechanism, Transmissions, and Automation in Design 106 (1984) 394–400.
[5] D.J. Gorman, R.K. Singhal, A superposition-Rayleigh–Ritz method for free vibration analysis of non-uniformly tensioned membrane, Journal of Sound and Vibration 162 (1993) 489–501.
[6] Ch-Y. Chia, Nonlinear Analysis of Plates, McGraw-Hill, New York, 1980.
[7] H.-N. Chu, G. Herrmann, Influence of large amplitudes on free flexural vibrations of rectangular elastic plates, Journal of Applied Mechanics 23 (1956) 532–540.
[8] J.M. Coan, U. Ill, Large-deflection theory for plates with small initial curvature loaded in edge compression, Journal of Applied Mechanics 18 (1951) 143–151.
[9] N. Yamaki, Postbuckling behavior of rectangular plates with small initial curvature loaded in edge compression, Journal of Applied Mechanics 26 (1959) 407–414.
[10] J. Crawford, S. Atluri, Non-linear vibration of a plate with initial stresses, Journal of Sound and Vibration 43 (1975) 117–129.
[11] J.R. Marin, N.C. Perkins, W.S. Vorus, Non-linear response of predeformed plates subject to harmonic in-plane edge loading, Journal of Sound and Vibration 176 (1994) 515–529.
[12] C. Pierre, E.H. Dowell, Astudy of dynamic instability of plate by an extended incremental harmonic balance method, Journal of Applied Mechanics 52 (1985) 1–5.
[13] A.H. Nayfeh, D.T. Mook, Non-linear Oscillations, Wiley, New York, 1979.
[14] S.P. Timoshenko, J.N. Goodier, Theory of Elasticity, 3rd Edition, McGraw-Hill, New York, 1970.
[15] L. Meirovitch, Analytical Methods in Vibrations, Macmillan, New York, 1967.
[16] D.E. Newland, An Introduction to Random Vibrations, Spectral and Wavelet Analysis, 3rd Edition, Longman, New York, 1993.